JOURNAL OF MATERIALS SCIENCE 27 (1992) 5982–5988

Modelling of transverse crack growth and saturation in cross-ply laminates

S. LACAZE
Renault Automobiles, 67 Rue des Bons Raisins, 92508 Rueil Malmaison Cedex, France
L. ANQUEZ
Avions Marcel Dassault, 92214 Saint-Cloud Cedex, France

A model of transverse cracking in cross-ply laminates is presented. The model describes the onset of cracking, the development of the number of cracks, the saturation phase of this damage mode and the final crack distribution, as well as the dependency of these phenomena on the 90° ply thickness. This analysis is based on an effective flaw size distribution and a non-linear interlaminar behaviour hypothesis. The theoretical prediction of the process and the saturation of cracking was well correlated with the experiments conducted on $[0_2/90_n]_s$ graphite/epoxy. However, there was considerable dispersion in the experimental results concerning the onset of cracking. Experimental work and part of the theoretical investigations were made at ONERA, 29 av. Division, Leclerc 92322, Chatillan, Cedex, France.

1. Choice of hypotheses

In the damage of composite materials under tensile loading, five modes of failure have been identified (Fig. 1): (1) transverse cracking, (2) delamination, (3) splitting, (4) fibre failure, and (5) fibre–matrix debonding. In the case of cross-ply laminates under uniaxial tensile loading, the first damage to appear in usual engineering composites is transverse cracking. Even if this phenomenon has a small influence on the global axial stiffness, it causes substantial reduction of compression and shear strengths [1], and it can be the cause of delamination in an unloading–reloading case [2, 3].

We propose here a simple model of transverse cracking from onset to the saturation phase which takes into account the "volume effect", i.e. the influence of the 90° layer thickness in the case of $[0_2/90_n]_s$ laminates.

Two hypotheses are necessary to allow us to describe this damage process: (1) a crack propagation criterion; (2) an interfacial behaviour hypothesis in the stress concentration area around the crack tip.

1.1. Crack propagation criterion

A common hypothesis is to assume the existence of microscopic flaws in the 90° layer (voids, microcracks due to residual thermal stresses, local heterogeneities due to an excess of fibres, etc.). The importance of each flaw is assumed to be quantified by a parameter a, which could be the size of an equivalent (same propagation characteristics) microcrack subjected to perpendicular loading and propagating in Mode I. The conditions for the validity of a Mode I fracture approach were given by Griffith [4] and are applicable here. To do this, one can use a classical fracture mechanics approach by using a criterion of propagation based on a critical value G_c of G, the energy release rate [5], or also on an equivalent critical value K_{Ic} of K_I, the stress intensity factor, where $K_I = \sigma_{90}(\pi a)^{1/2}$.

Therefore, relate any flaw of size a can be related to a critical value of stress at which the crack propagates by $\sigma_{90} = K_{Ic}/(\pi a)^{1/2}$. This equation relates a given statistical distribution of defect size to a given statistical distribution of crack propagation stresses, $f(\sigma_{90})$. Considering that failure of a chain occurs when its weakest link fails, and if we assume a statistical distribution of failure stresses $f(\sigma)$, it can easily be shown, using the density function of the minimum of independent random variables, that the probability for a link of volume dV, to fail during loading from 0 to σ is [6]:

$$P(\sigma) = 1 - \exp[-f(\sigma)dV] \quad (1)$$

The choice of $f(\sigma)$ is a matter of discussion. The most commonly used function is a two parameter Weibull distribution $f(\sigma) = (\sigma/\sigma_0)^a$ [6–8], or a normal distribution [5]. However, it has been shown that these functions are not satisfactory in some circumstances [6]. For each material we must choose a function which can take into account fibre, matrix, and interface properties as well as the manufacturing process. Here, a three-parameter Weibull function $f(\sigma) = [(\sigma - \sigma_u)/\sigma_0]^a$ and a two-parameter Gumbell function $f(\sigma) = \exp[-\beta(\sigma - \sigma_u)]$ are used. Both have given satisfactory results even if the Weibull function seems easier to use for the experimental determination of the parameters and appears to be more flexible (by having three parameters instead of two).

1.2. Interfacial behaviour hypothesis

The hypotheses proposed for modelling the stress distribution around cracks are widely inspired by the

0022–2461 © *1992 Chapman & Hall*

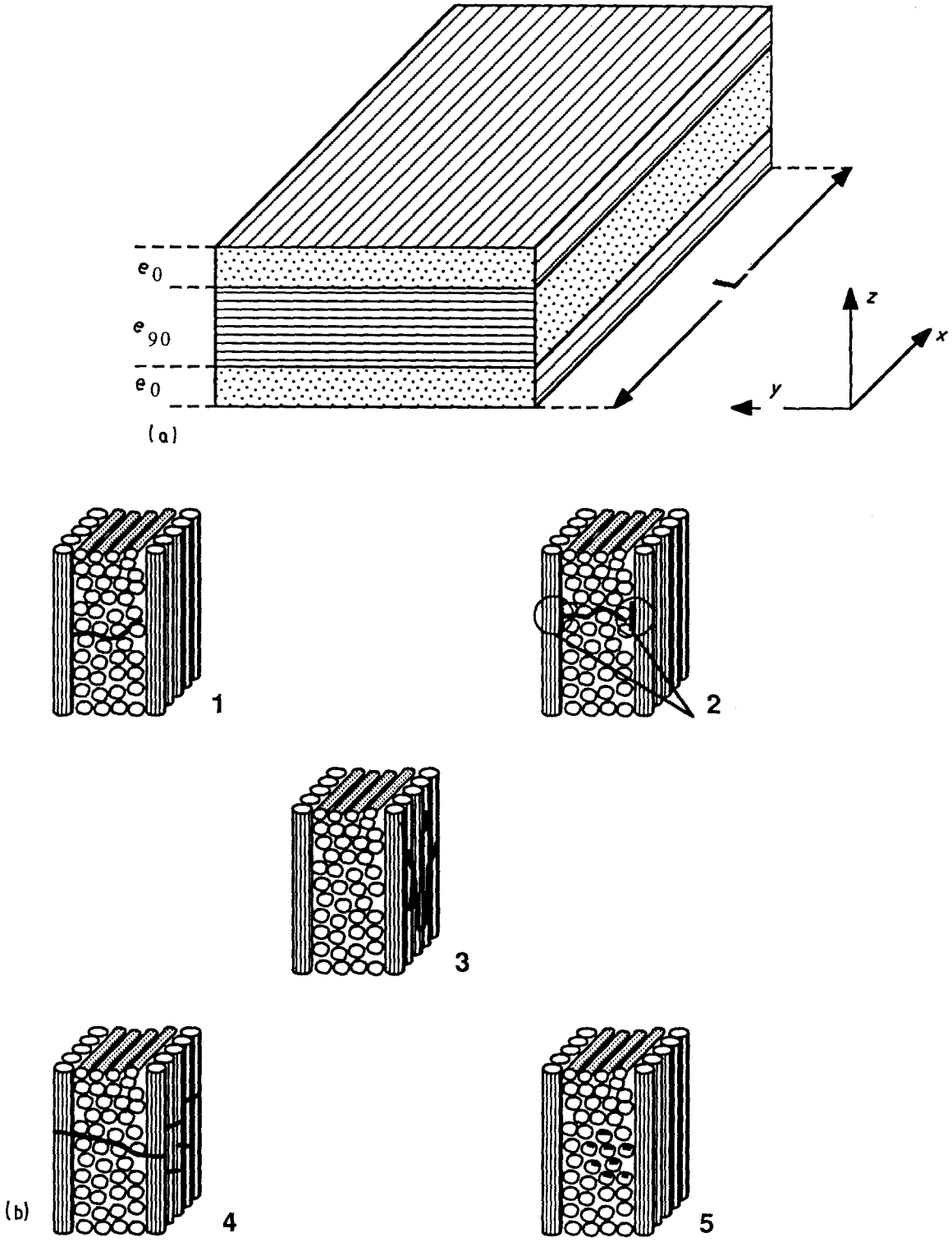

Figure 1 (a) Nomenclature and axes of reference. (b) Modes of failure of a cross-ply laminate. 1, Transverse cracking; 2, delamination; 3, splitting; 4, fibre failure; 5, fibre–matrix debonding.

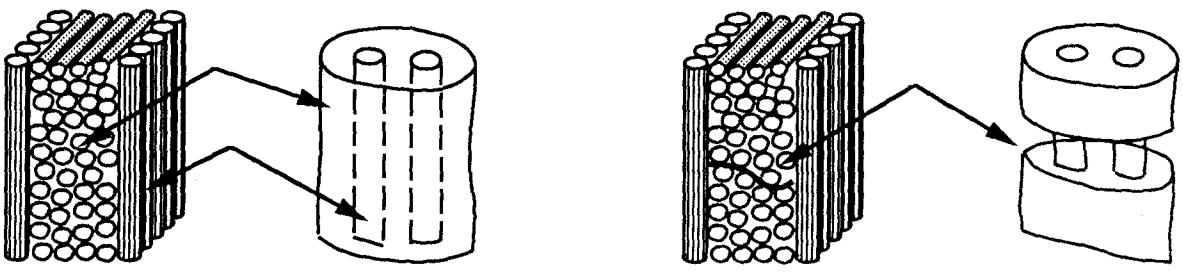

Figure 2 Analogy between a unidirectional composite and a laminated composite.

work of Aveston *et al.* [9, 10] on composites made of a brittle matrix reinforced by unidirectional fibres.

One can apply these hypotheses to cross-ply laminates by considering each ply as a homogeneous equivalent material [11]. This analogy can be represented by Fig. 2.

The first approach of Aveston *et al.* [9] was to consider the matrix and the fibre in the neighbourhood of a crack as unbonded. The word unbonded means there is no connection between elastic displacements of fibre and matrix, and both interfacial debonding and lamina sliding will occur when an upper shear stress limit is reached.

In their second approach [10], the matrix remains bonded and its behaviour is fully elastic. This is an extension of Cox's elastic shear lag analysis [12]. It has been applied to cross-ply laminates by Garret and Bailey [13], Parvizi *et al.* [14] and Manders *et al.* [6]. Peters [7], and Chou and Peters [8] have also used a similar approach with the additional assumption that a limited interfacial area exists and supports all the shear stress. However, the saturation process and the volume effect remain both difficult to describe because of the complexity of the axial stress distribution [7].

Aveston and Kelly [10] have found two main limits in their first approach: (1) the physical justification of the interfacial sliding hypothesis (at constant shear stress τ_c), and (2) the problem of non-aligned fibres. The second limit does not apply in the case of laminates because they consist of macroscopic layers instead of microscopic fibres. Therefore, the parallelism can be assumed as perfect. The first approach, has been successfully used in unidirectional ceramic composites and in steel-reinforced epoxy composites [15], where the diameter of the fibre is not small and the fibre volume fraction is not high. However, the interfacial behaviour of laminates is much more complex. Figs 3 and 4 are microscopic pictures taken after the surface was treated with an opaque substance. Fig. 3 shows an area of interfacial sliding which may be due to local delamination as well as plastic behaviour of the matrix as the interface. Fig. 4 shows local plasticity and fibre–matrix debonding near the crack tip. Such debonding has been clearly observed by Bailey and Parvizi [16] for glass–epoxy laminates. Because the interfacial strength is lower for graphite–epoxy, debonding does probably play an important role in the 90° layer.

The major assumption of this paper is to use the interfacial sliding hypothesis at constant shear stress, τ_c, to model these three energy dissipation phenomena (sliding, debonding and plasticity).

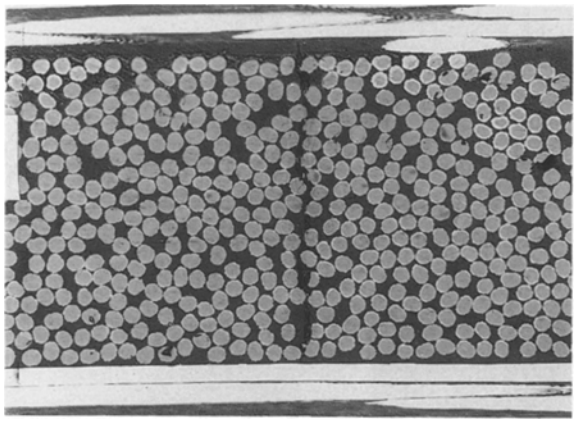

Figure 3 Interfacial sliding at the interface around the crack tip.

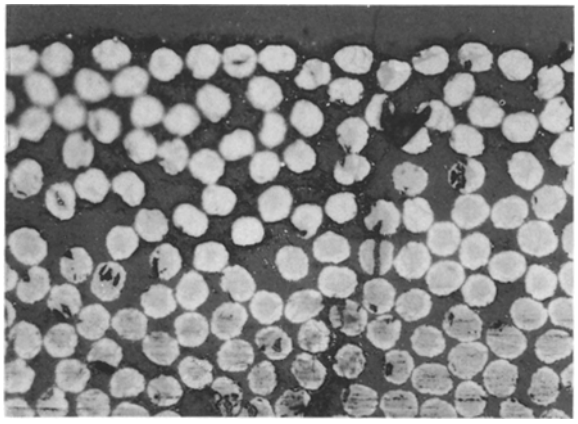

Figure 4 Fibre–matrix debonding near the crack tip (ONERA picture).

2. Stress analysis

2.1. The 90° ply

To assess the stress distribution around the crack with the assumption of interfacial sliding, a finite difference numerical analysis was conducted. The finite difference technique is easier to use to break links between nodes at the interface when $\tau_{xz} = \tau_c$ is reached. This numerical simulation describes the progression of interfacial sliding as well as the distribution of shear

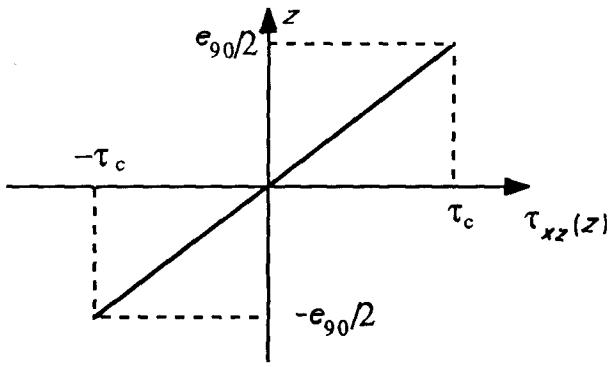

Figure 5 $\tau_{xz}(z)$ near the crack in the 90° layer.

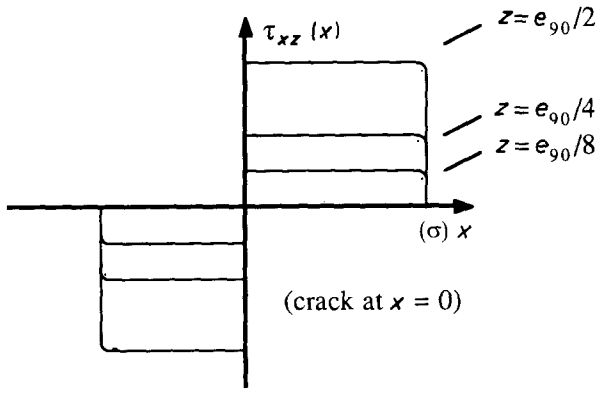

Figure 6 $\tau_{xz}(x)$ in the 90° layer.

stress in the 90° ply. These results are shown in Figs 5 and 6. The shapes of these curves are a consequence of the sliding hypothesis. The τ_{xz} distribution along the x-axis clearly shows the existence of two distinct zones: (1) a non-perturbed area where the condition of static equilibrium gives $\sigma_x = \sigma_\infty$ and $\tau_{xz} = 0$; (2) a perturbed area around the crack. It's length is denoted $2l(\sigma_\infty)$.

To assess σ_x and $l(\sigma_\infty)$, where σ_∞ denotes the value of axial stress in the 90° layer far from the crack, one can use a plane strain analysis and assume that the state of stress does not depend on y and also that ε_y = constant and $\gamma_{xy} = \gamma_{yz} = 0$. For an orthotropic material, these assumptions lead to $\tau_{xy} = \tau_{yz} = 0$. Then, the equilibrium equations become

$$\partial\sigma_x/\partial x + \partial\tau_{xz}/\partial z = 0 \qquad (2a)$$

and

$$\partial\tau_{xz}/\partial x + \partial\sigma_z/\partial z = 0 \qquad (2b)$$

In the damaged zone, we have $\partial\tau_{xz}/\partial x = 2\tau_c/e_{90}$ (see Fig. 5). Hence $\partial\sigma_x/\partial x = -2\tau_c/e_{90}$ and then

$$\sigma_x = -2\tau_c x/e_{90} \quad \text{for } x \in [0, l(\sigma_\infty)] \text{ (see Fig. 7).} \qquad (3)$$

The boundary condition $\sigma_x = \sigma_\infty$ at the limit of the damaged area leads to

$$l(\sigma_\infty) = \sigma_\infty e_{90}/(2\tau_c) \qquad (4)$$

The equation of the free surface of the crack comes from $\gamma_{xz} = \partial u/\partial z + \partial w/\partial x$ and if we neglect $\partial w/\partial x$, we have

$$\begin{aligned} \partial u/\partial z &= \gamma_{xz} \\ &= \tau_{xz}/G_{23} \\ &= 2\tau_c z/(G_{23} e_{90}) \\ \Rightarrow u(x, z) &= \tau_c z^2/(G_{23} e_{90}) + u(x, 0) \end{aligned} \qquad (5)$$

(see Fig. 8).

2.2. The 0° ply

In a similar manner, we obtain the distribution of stresses in the 0° plies as shown in Fig. 9. The reduction of stiffness in the 90° layer is supported by the 0° layer, but the large difference of Young's modulus between the two layers is the reason why, in $[0_2/90_2]_s$ laminates, $\Delta\sigma_x/\sigma_x$ is only 0.2%.

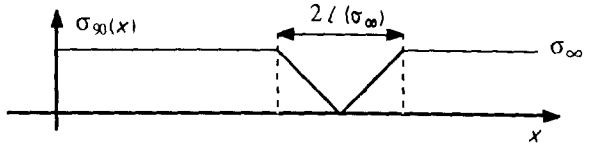

Figure 7 $\sigma_x(x)$ around a crack.

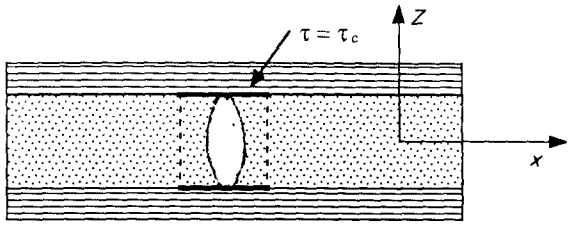

Figure 8 Free surface of the crack and sliding area.

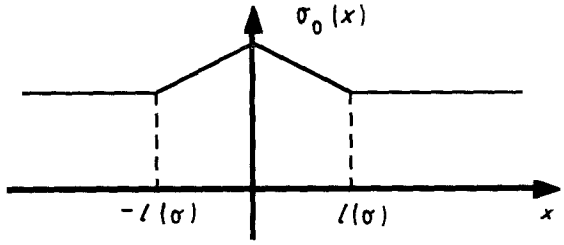

Figure 9 $\sigma_x(x)$ around a crack in the the 0° layer.

3. Multi-cracking process

3.1. Axial stress distribution during the loading

From the previous stress analysis, we can deduce $\sigma_x(x)$ in the 90° ply if we know the location of the cracks (Fig. 10). When the load σ_∞ is increased by $d\sigma_\infty$, the stress distribution around the crack is not modified because the slope of σ_x in this area (i.e. $2\tau_c/e_{90}$) is independent of the loading (Fig. 10). The damaged area of length $2l(\sigma_\infty)$ around the crack can therefore be considered as inactive because, as the stress σ_∞ increases, the local stress intensity factor remains constant and smaller than K_c, otherwise another crack would have already propagated. The new cracks will appear only in the active area. The length of this area as a function of σ_∞ will be assessed in section 3.2.

3.2. Active fissurable length

To assess the development of cracks, we need to be precise concerning the statistics of very critical failure stresses.

Let Ω be the set of all the uniaxial tensile loading experiments on originally undamaged material; one specific experiment of the set Ω is denoted by ω.

Let $X(\omega)$: $\Omega \to R^+$, be the random variable which relates a specific experiment ω to the value of stress $\sigma = X(\omega)$ at which the first crack propagates in the composite sample. As mentioned earlier, according to the principle of the weakest link in a chain, the distribution function of $X(\omega)$ for a statistical repartition of failure stresses $f(\sigma)$ is [6]

$$P(\sigma) = P[X(\omega) \leq \sigma] = 1 - \exp[-\int f(\sigma) dV] \qquad (6)$$

In the case of a three-parameter Weibull distribution, we obtain

$$P(\sigma) = 1 - \exp(-\int [(\sigma - \sigma_u)/\sigma_0)^a dV] \quad \text{for } \sigma \geq \sigma_u \qquad (7a)$$

$$P(\sigma) = 0 \quad \text{for } \sigma < \sigma_u \qquad (7b)$$

The probability of crack propagation between

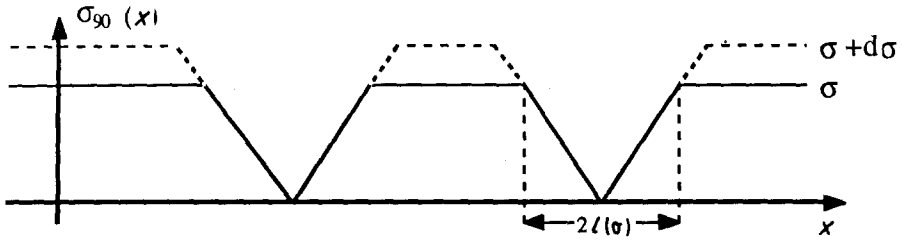

Figure 10 Variation of the axial stress distribution during the loading.

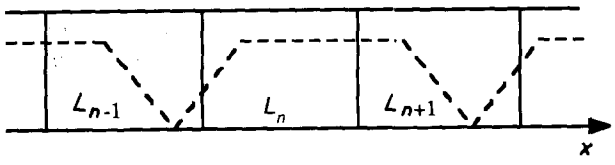

Figure 11 The crack in link L_{n-1} reduces the active length of the link L_n while the crack in the link L_{n+1} does not.

σ and $\sigma + d\sigma$ is obtained by the density of the law

$$p(\sigma)d\sigma = P'(\sigma)d\sigma = -\int[(\sigma - \sigma_u)/\sigma_0]^{a-1} (a/\sigma_0)dV\exp[-\int[(\sigma - \sigma_u)/\sigma_0]^a dV]d\sigma \quad (8)$$

As mentioned earlier, when the number of cracks increases, the integration area, i.e. the "active fissurable length" (a.f.l.), decreases. Let us divide the composite bar into links of length $2l(\sigma)$ I. If $P(\sigma)$ becomes the probability for a such link to fail before σ, we can show by a statistical analysis that the average active length on the link is reduced by a factor $\alpha[P(\sigma)]$ because of the perturbation of the neighbouring cracks (Fig. 11) and we have

$$\langle \text{a.f.l.} \rangle = \alpha[P(\sigma)]2l(\sigma) \quad (9)$$

where

$$\alpha(P) = \{(1 - P)(1 - P/4) + (P/4)[P^2(7/8 - (\ln 2)/2) + P(\ln 2 - 3/2) + 1]\} \quad (10)$$

3.3. Crack growth as a function of σ

Applying Equation 8 to the case of a simple link instead of the whole bar, we have the differential equation

$$p(\sigma) = P'(\sigma) = [(\sigma - \sigma_u)/\sigma_0]^{a-1} \alpha(P)a\sigma (e_{90}/\tau_c)\exp\{-[(\sigma - \sigma_u)/\sigma_0]^a \alpha(P)\sigma e_{90}/\tau_c\} \quad (11)$$

This equation provides an explicit expression

$$P_{n+1} - P_n = [(n\Delta\sigma - \sigma_u)/\sigma_0]^{a-1} \alpha(P_n)an\Delta\sigma^2 (e_{90}/\tau_c)\exp\{-[(n\Delta\sigma - \sigma_u)/\sigma_0]^a \alpha(P_n)n\Delta\sigma e_{90}/\tau_c\} \quad (12)$$

Knowing $P(\sigma)$, we can obtain

$$N(\sigma) = P(\sigma)L/[2l(\sigma)] \quad (13)$$

where $N(\sigma)$ is the number of cracks at a given stress, σ. The results are shown in Fig. 12 for different values of e_{90}. From the curve we can deduce the following significant results: (i) the value of σ for the first crack (solution of $N(\sigma) = 1$); (ii) the number of cracks at saturation (maximum of $N(\sigma)$); (iii) the stress σ_{sat} at saturation ($\sigma \geq \sigma_{sat} \Rightarrow N(\sigma) = \text{constant}$).

4. Correlation with experiments

Experiments have been conducted on graphite–epoxy $[0_2/90_n]_s$ laminates with $n = 1, 2, 4$. The results of experiments for $n = 2$ have been used to determine the three Weibull and two Gumbel parameters. The cracks were recorded by acoustic emission. Each com-

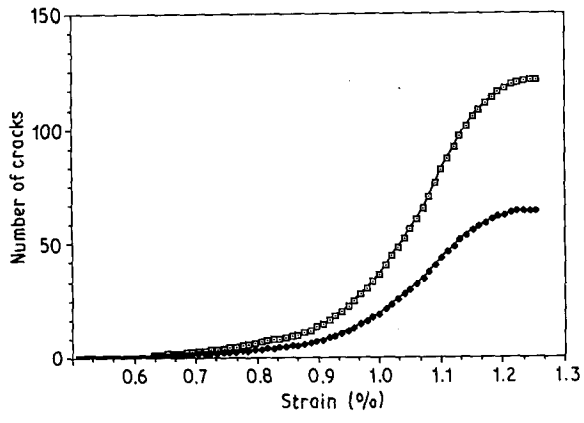

Figure 12 The theoretical number of cracks during the loading experiment. (□) $n = 2$, (◆) $n = 4$.

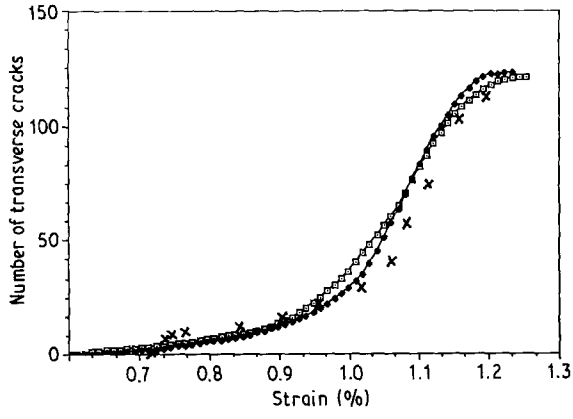

Figure 13 Comparison between (×) experimental and (□, ◆) theoretical crack propagation. (□) Weibull parameter, (◆) Gumbel parameter.

posite specimen was examined at least once during loading (by X-rays) to check the validity of the acoustic emission recordings and to determine the crack spacing. Excellent correlation was found.

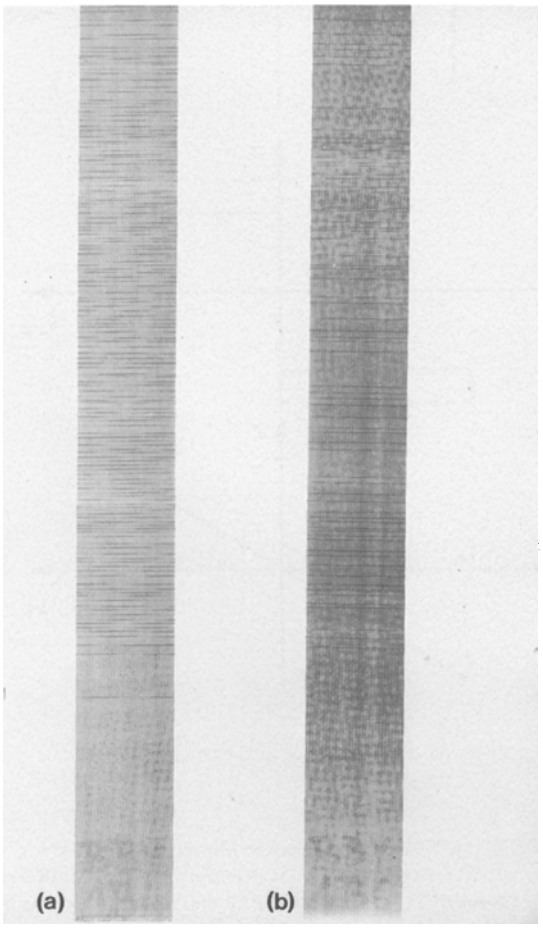

Figure 14 (Top view) Cracking distribution close to saturation for (a) $n = 2$ and (b) $n = 4$ (X-ray picture).

TABLE I Number of cracks at saturation

No. of layers	Calculation	Experiments
2	229	240
4	122	130
8	65	65

TABLE II Strain at saturation (%)

No. of layers	Calculation	Experiments
2	1.48	1.5
4	1.26	1.25
8	1.06	1.25

The next step lay in the application of the results of our analysis for $n = 1, 2$ and 4 to predict the onset of cracking, the crack growth, and the saturation phase. It can be seen that the shapes of the growth curves fit satisfactorily (Fig. 13). The most satisfactory result is the prediction of the number and the spatial repartition of cracks at saturation – the crack spacing density appears to be inversely proportional to the ply thickness (Table I). For $n = 4$, the results have been extrapolated because some areas were not saturated at 0° ply failure.

Experimental determination of saturation is difficult and can only be approximate (Table II). It can be said however, that the saturation stress decreases when the ply thickness increases.

The most difficult result to analyse is the onset of cracking, because the dispersion of the experimental results does not allow one to draw any conclusion about the ply thickness effect. The model shows a slight dependence of this effect on the onset of cracking (Table III). (The first crack is said to propagate when a probability of 1/2 is met). Wang and Crossman [2], and Parvizi *et al.* [14] found the ply thickness to have a strong effect for very thin plies but almost none above a reasonable thickness of the transverse ply ($e_{90} \geq e_0$). The present experiments were conducted only for the case $e_{90} \geq e_0$.

The delaminations observed in the experiments (Fig. 14) are not edge delaminations as encountered by Wang *et al.* [5] but delaminations along the transverse cracks. This observation verifies the interfacial behaviour assumptions used in this model.

5. Conclusion

The model presented in this paper correlates well with experiments, especially for the volume effect on crack spacing and number as well as for the description of crack growth. However, its validity has to be checked for very thin transverse layers.

The choice of a probability distribution of failures can be made in other ways, but a Weibull function is probably the most convenient. Finally, the interfacial sliding hypothesis seems a good model of the complexity of the interfacial behaviour but is not an explanation in itself. The physical interpretation that we have presented should be verified by a microscopic study of the interface around the crack tip.

Appendix

Let us show a comparison between shear stress distribution assumptions $\tau_{xz}(z)$, in shear lag analysis, modified shear lag analysis, and unbonded analysis. From

TABLE III Strain (%) at the onset of cracking

No. of layers	Calculation	Experiments	Experimental average
2	0.84	0.83, 1.00, 1.01	0.95
4	0.78	0.61, 0.75, 0.79, 0.80, 0.97	0.82
8	0.71	0.75, 0.80, 0.85, 0.94	0.84

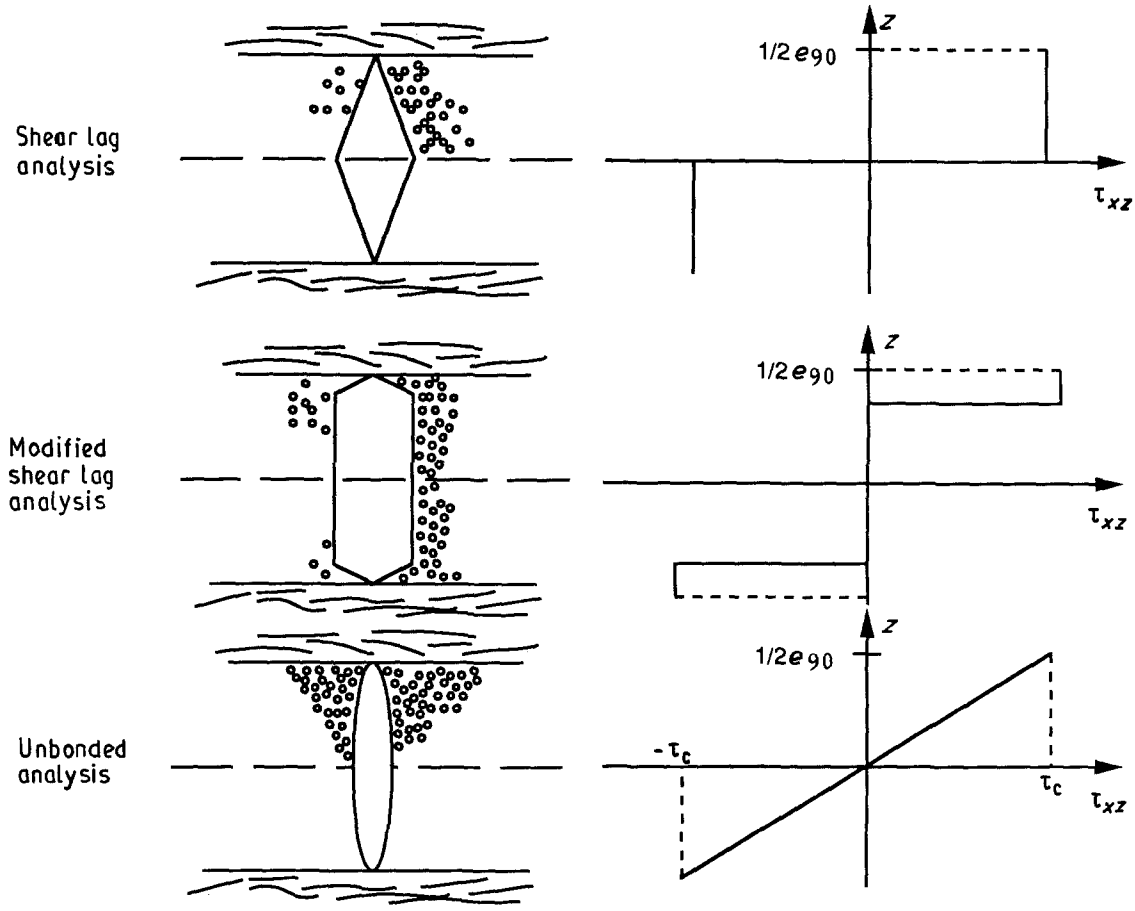

Figure A1 Different shear stress distribution assumptions and their consequences on the free surface of the crack.

the stress distribution $\tau_{xz}(z)$ and Equation 5, one can deduce the equation of the free surface of the crack:

$$u(x, z) = \int (\tau_{xz}(z)/G)dz + u(x, 0) \qquad (A1)$$

The results for the three cases are shown in Fig. A1.

References

1. C. C. CHAMIS and T. L. SULLIVAN, "In situ ply strength: An initial assessment", NASA TM-73771 (1978).
2. A. S. D. WANG and F. W. CROSSMAN, *J. Compos. Mater. Suppl.* **14** (1980) 71.
3. K. L. REIFSNIDER, W. W. STINCHCOMB, E. G. HENNECKE and J. C. DUKE, "Fatigue damage strength relationships in composite laminates", AFWAL-TR-83-3084, Air Force Wright Aeronautical laboratories, September 1983.
4. A. A. GRIFFITH, in "Proceedings of the First International Congress on Applied Mechanics", Delft, Holland (1924) p. 55.
5. A. S. D. WANG, P. C. CHOU and S. C. LEI, *J. Compos. Mater.* **18** (1984) 239.
6. P. W. MANDERS, T. W. CHOU, F. R. JONES and J. W. ROCK, *J. Mater. Sci.* **18** (1983) 2876.
7. W. M. PETERS, *J. Compos. Mater.* **18** (1984) 549.
8. T. W. CHOU and P. W. M. PETERS, *Composites* **18** (1987) 40.
9. J. AVESTON, G. A. COOPER and A. KELLY, "The properties of fibre composites" Conference proceedings, National Physical Laboratory (IPC Science and Technology Press, 1971) Paper I, p. 15.
10. J. AVESTON and A. KELLY, *J. Mater. Sci.* **8** (1973) 352.
11. S. W. TSAI and H. T. HAHN, "Introduction to Composite Materials" (Technomic, 1980).
12. H. L. COX, *Brit. J. Appl. Phys.* **3** (1952) 72.
13. K. W. GARRET and J. E. BAILEY, *J. Mater. Sci.* **12** (1977) 157.
14. A. PARVIZI, K. W. GARRET and J. E. BAILEY, *ibid.* **13** (1978) 195.
15. G. A. COOPER and J. M. SILLWOOD, *J. Mater. Sci.* **7** (1972) 325.
16. J. E. BAILEY and A. PARVIZI, *ibid.* **16** (1981) 649.

Received 5 April 1990
and accepted 1 May 1991.